Supporting Information

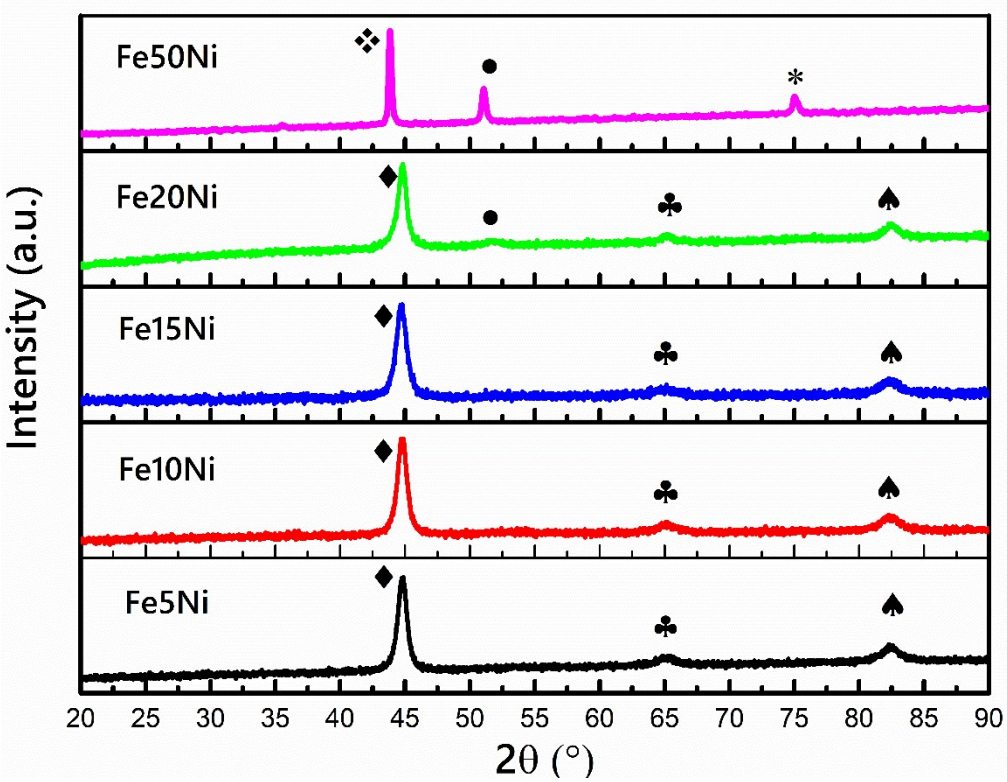

Fig.S 1. XRD results of synthesized Fe-Ni powders by mechanical alloying at different weight ratio.

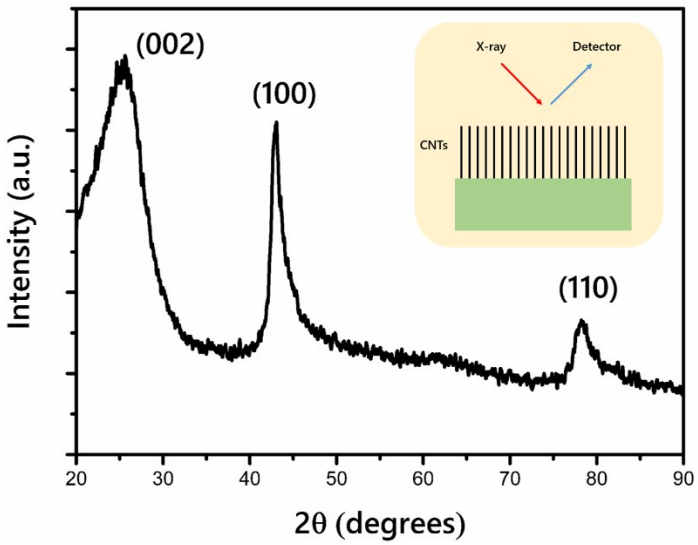

Fig.S 2. XRD pattern of VACNTs.

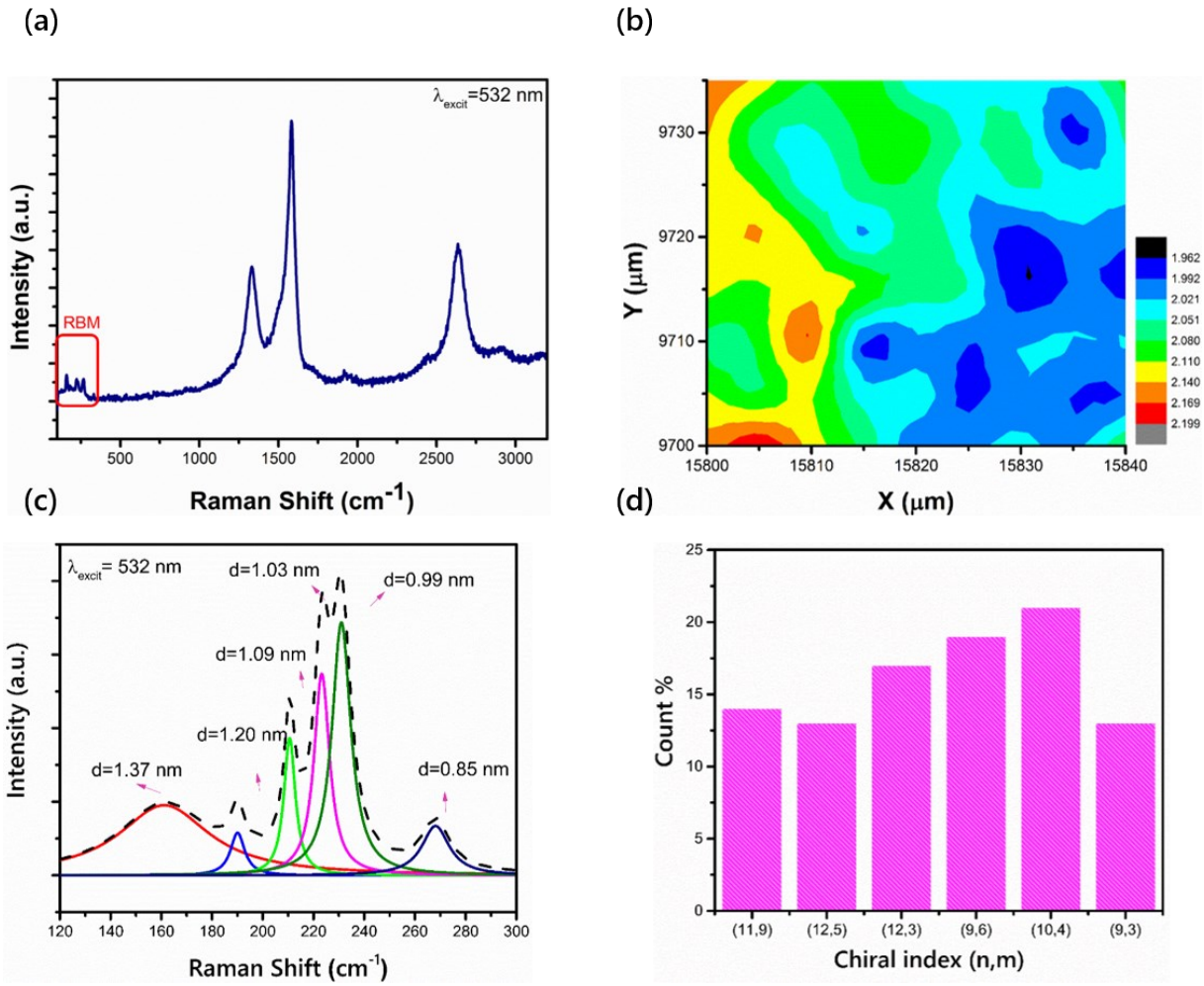

Fig.S 3. The results of VACNTs synthesized on the pure-Fe nanoparticles (a) full Raman spectra, (b) Raman mapping result for 1600 μm^2 area, (c) RBM peaks fitted with Lorentz and calculation of VACNTs innermost diameter, (d) the calculation and distribution of chiral index of VACNTs with electronic bands.

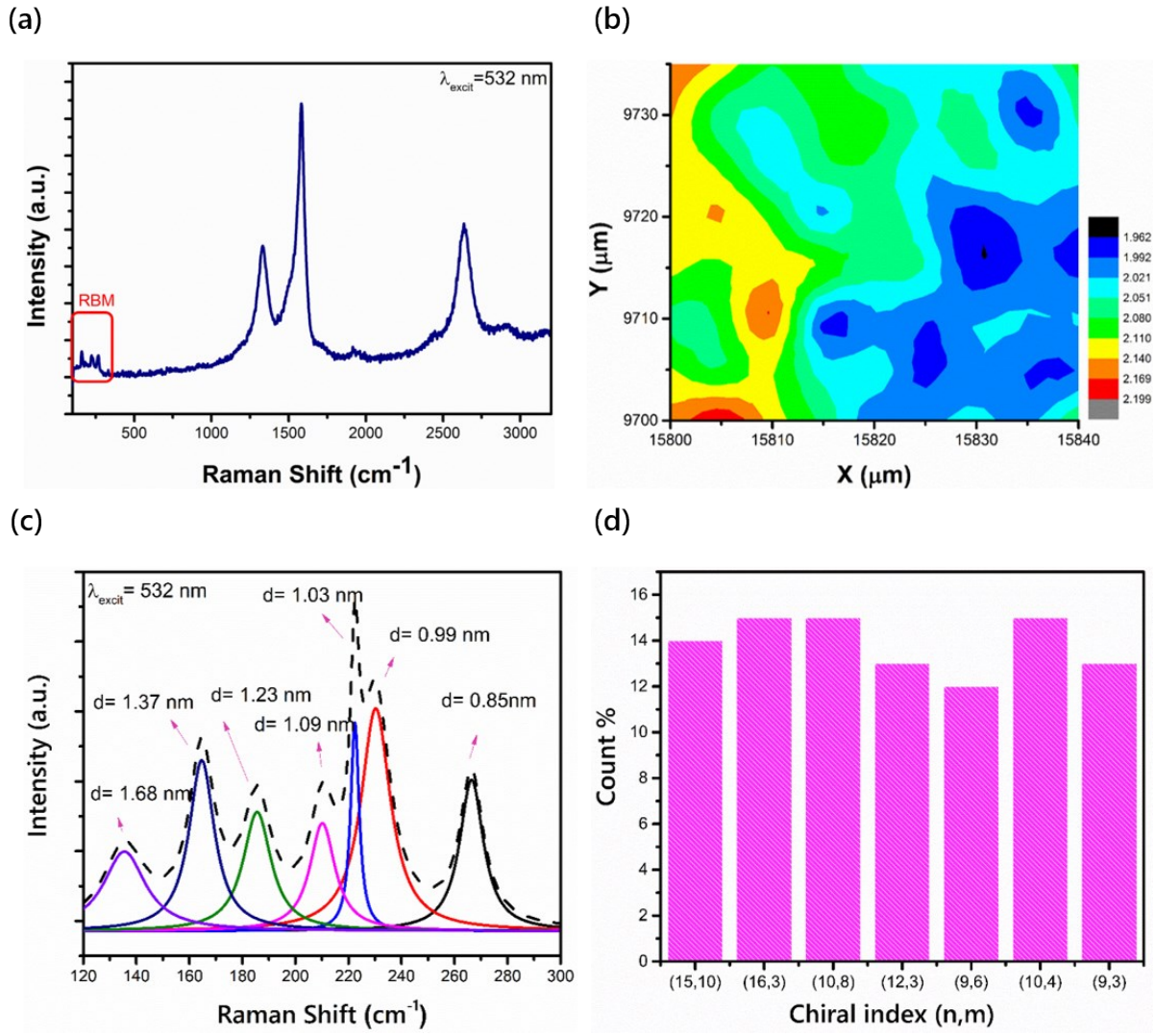

Fig.S 4. The results of VACNTs synthesized on the Fe5Ni nanoparticles (a) full Raman spectra, (b) Raman mapping result for 1600 μm^2 area, (c) RBM peaks fitted with Lorentz and calculation of VACNTs innermost diameter, (d) the calculation and distribution of chiral index of VACNTs with electronic bands.

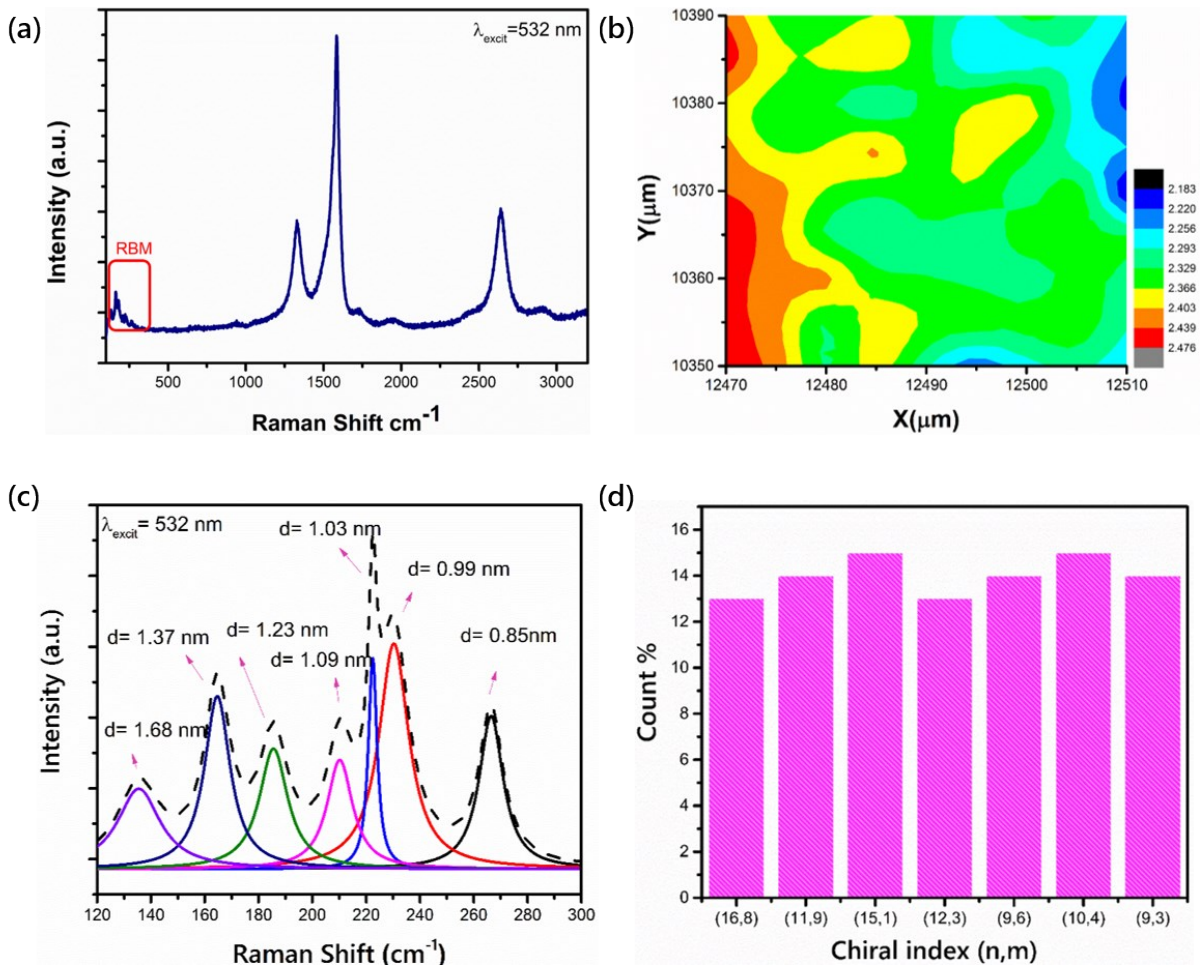

Fig.S 5. The results of VACNTs synthesized on the Fe10Ni nanoparticles (a) full Raman spectra, (b) Raman mapping result for 1600 μm^2 area, (c) RBM peaks fitted with Lorentz and calculation of VACNTs innermost diameter, (d) the calculation and distribution of chiral index of VACNTs with electronic bands.

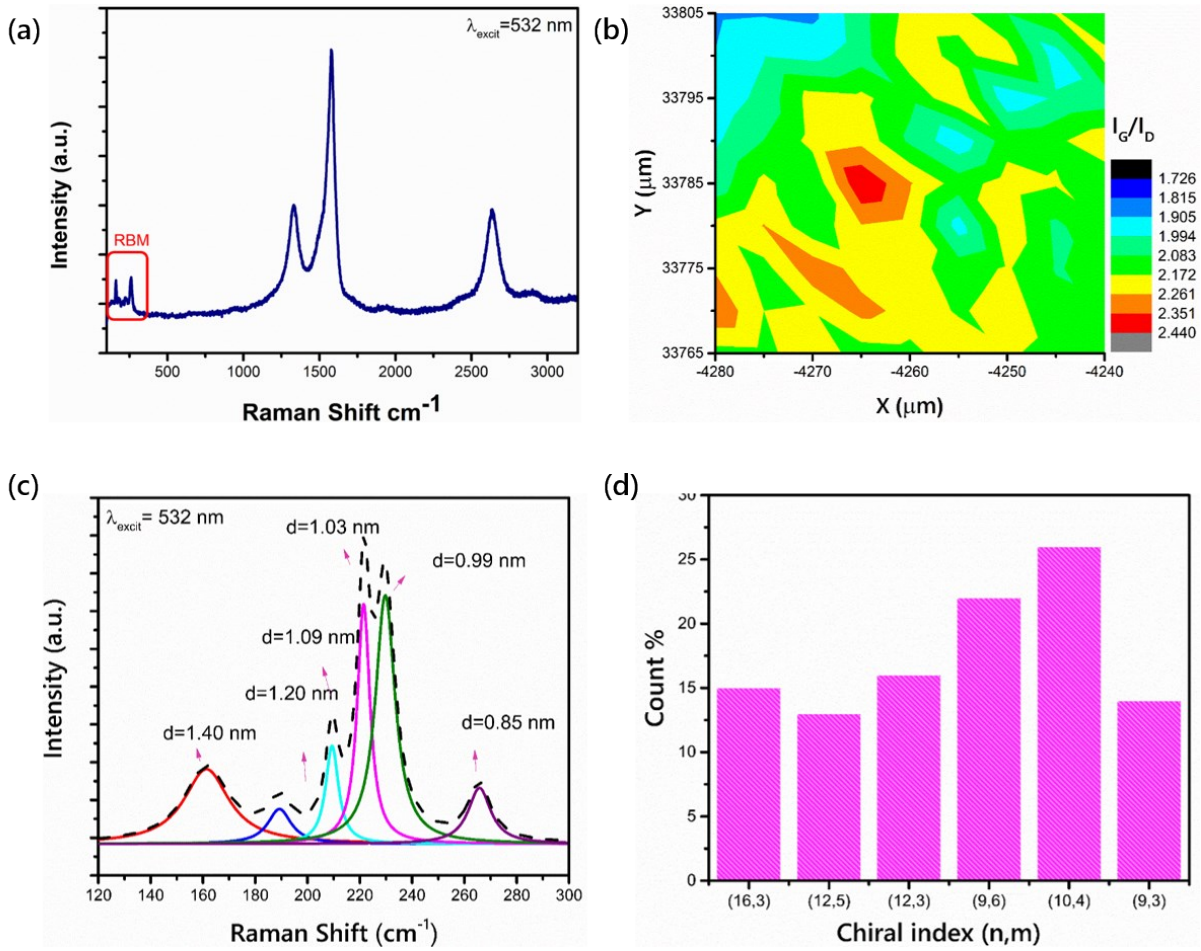

Fig.S 6. The results of VACNTs synthesized on the Fe15Ni nanoparticles (a) full Raman spectra, (b) Raman mapping result for 1600 μm^2 area, (c) RBM peaks fitted with Lorentz and calculation of VACNTs innermost diameter, (d) the calculation and distribution of chiral index of VACNTs with electronic bands.

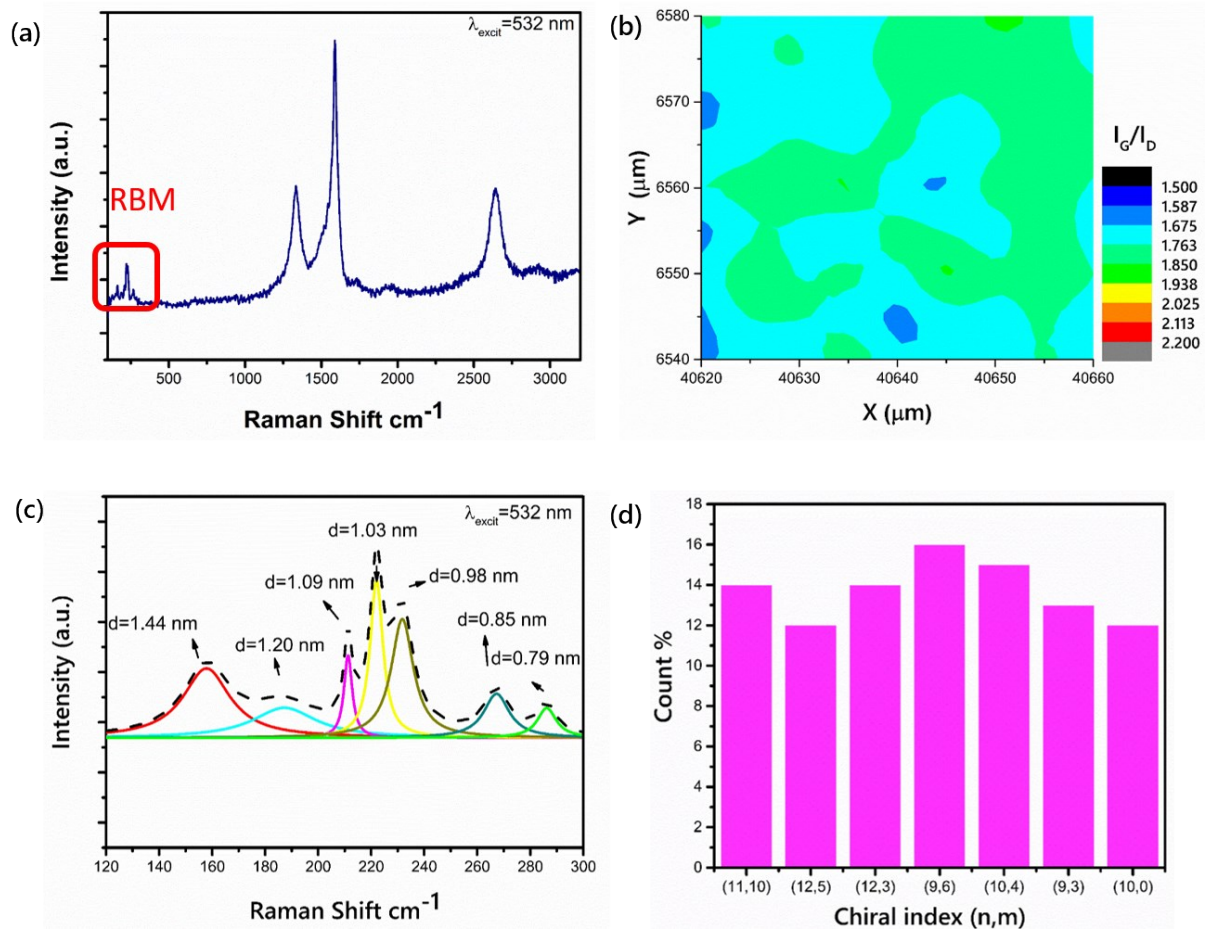

Fig.S 7. The results of VACNTs synthesized on the Fe20Ni nanoparticles (a) full Raman spectra, (b) Raman mapping result for 1600 μm^2 area, (c) RBM peaks fitted with Lorentz and calculation of VACNTs innermost diameter, (d) the calculation and distribution of chiral index of VACNTs with electronic bands.

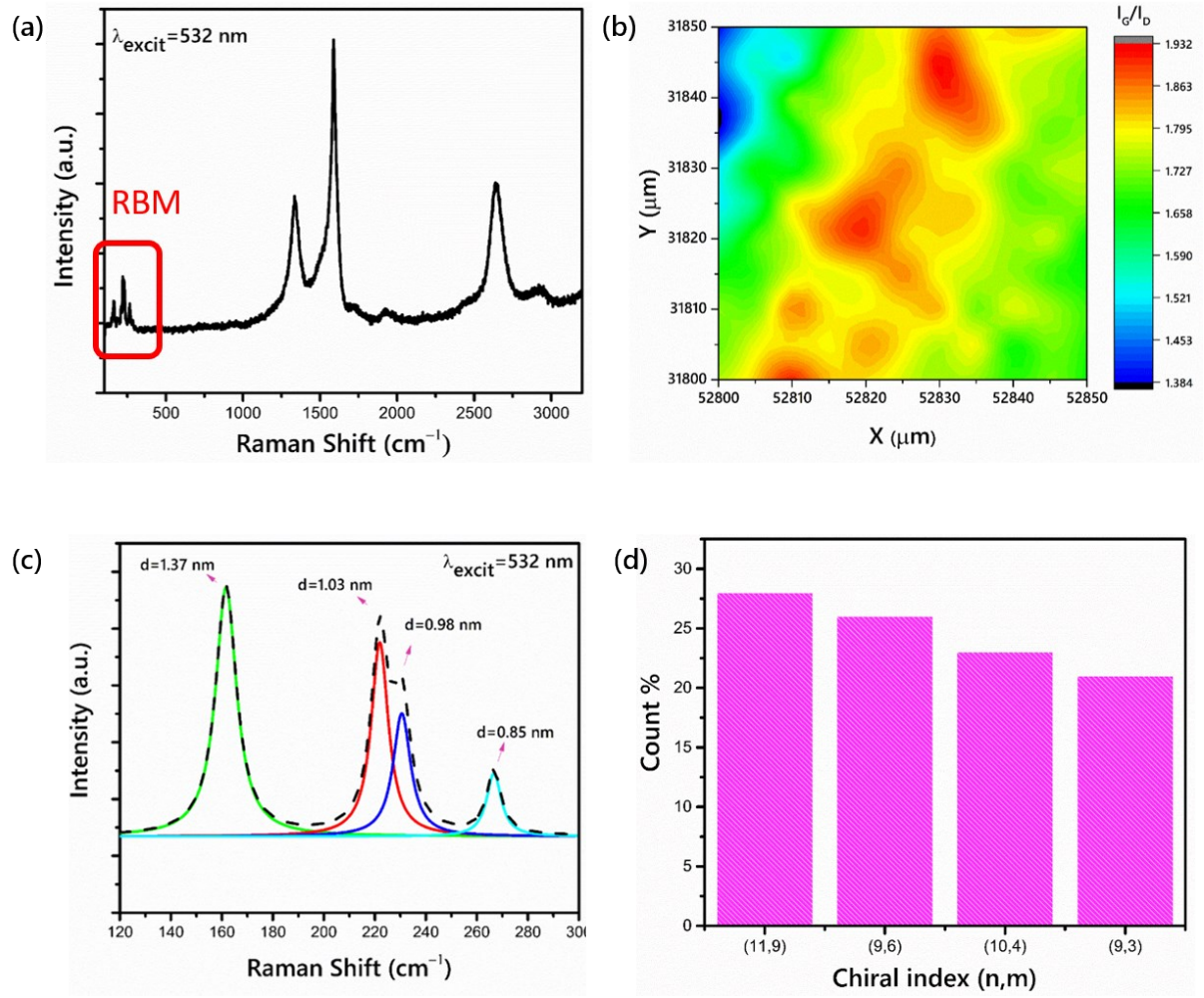

Fig.S 8. The results of VACNTs synthesized on the Fe50Ni nanoparticles (a) full Raman spectra, (b) Raman mapping result for 1600 μm^2 area, (c) RBM peaks fitted with Lorentz and calculation of VACNTs innermost diameter, (d) the calculation and distribution of chiral index of VACNTs with electronic bands.

Table S 1: RBM shift of synthesized VACNTs by Fe and Fe-Ni alloy combinations for green laser spot (2.33 eV, 532 nm) used in all calculations (ω_{RBM} : Mean value from 121 spectra) [35,51,52].

Catalyst type	ω_{RBM} (cm^{-1})	(n, m)	Family (2n+m)	d (nm)	S or M	E_{GAP}	E_{ii}	Electronic band
Fe-only	165	(11,9)	31	1.37	S	0.61	1.81	○
	187	(12,5)	29	1.20	S	0.70	2.08	○
	208	(12,3)	27	1.09	M	-	2.29	▲
	220	(9,6)	24	1.03	M	-	2.41	▲
	229	(10,4)	24	0.99	M	-	2.52	▲
	267	(9,3)	21	0.85	M	-	2.91	▲
Fe5Ni	131	(15,10)	40	1.73	S	0.50	1.93	▫
	162	(16,3)	35	1.40	S	0.60	1.78	○
	182	(10,8)	28	1.24	S	0.67	2.02	○
	208	(12,3)	27	1.09	M	-	2.29	▲
	220	(9,6)	24	1.03	M	-	2.41	▲
	229	(10,4)	24	0.99	M	-	2.52	▲
	267	(9,3)	21	0.85	M	-	2.91	▲
Fe10Ni	135	(16,8)	40	1.68	S	0.49	1.98	▫
	164	(11,9)	31	1.37	S	0.61	1.81	○
	185	(15,1)	31	1.23	S	0.68	2.03	○
	208	(12,3)	27	1.09	M	-	2.29	▲
	220	(9,6)	24	1.03	M	-	2.41	▲
	230	(10,4)	24	0.99	M	-	2.52	▲
	266	(9,3)	21	0.85	M	-	2.91	▲
Fe15Ni	162	(16,3)	35	1.40	S	0.60	1.78	○
	187	(12,5)	29	1.20	S	0.70	2.08	○
	208.	(12,3)	27	1.09	M	-	2.29	▲
	220	(9,6)	24	1.03	M	-	2.41	▲
	229	(10,4)	24	0.99	M	-	2.52	▲
	267	(9,3)	21	0.85	M	-	2.91	▲
Fe20Ni	157	(11,10)	32	1.44	S	0.58	1.73	○
	188	(12,5)	29	1.20	S	0.70	2.08	○
	210	(12,3)	27	1.09	M	-	2.29	▲
	221	(9,6)	24	1.03	M	-	2.41	▲
	231	(10,4)	24	0.98	M	-	2.52	▲
	267	(9,3)	21	0.85	M	-	2.91	▲
	286	(10,0)	20	0.79	S	1.06	2.11	▲
Fe50Ni	165	(11,9)	31	1.37	S	0.61	1.81	○
	220	(9,6)	24	1.03	M	-	2.41	▲
	229	(10,4)	24	0.98	M	-	2.52	▲
	267	(9,3)	21	0.85	M	-	2.91	▲
	$M_{11} = 6i\gamma_0/d_t$, $S_{22} = 4i\gamma_0/d_t$, $S_{33} = 8i\gamma_0/d_t$							M_{11}: ▲ S_{22}: • S_{33}: ○ S_{44}: ▫
	$S_{44} = 16i\gamma_0/d_t$, $E_{GAP} = 0.84/d_t$							

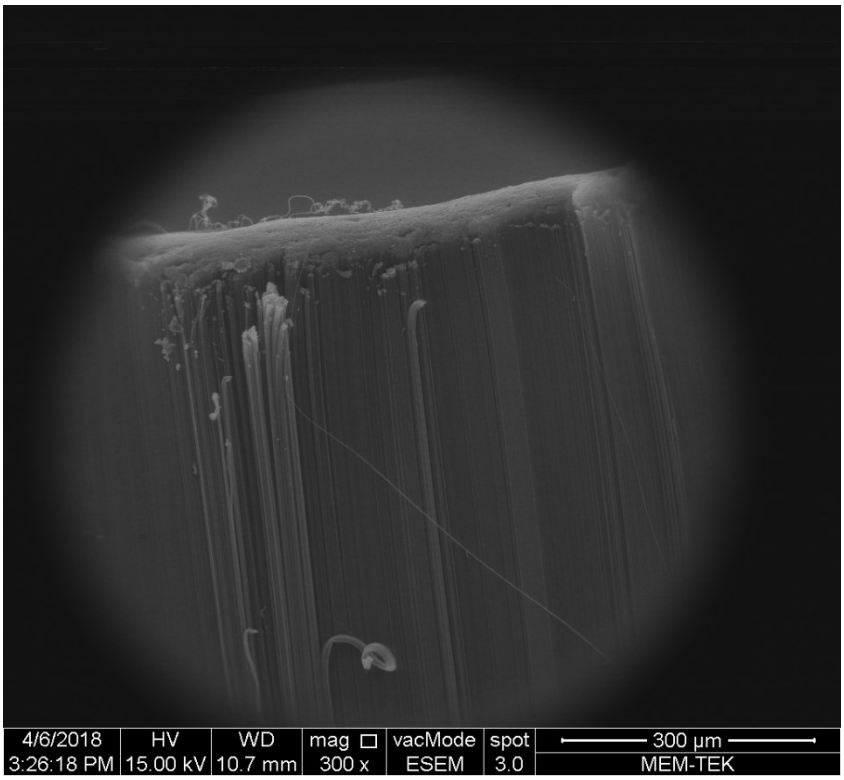

Fig.S 9: SEM image from top of VACNTs synthesized on the pure-Fe.

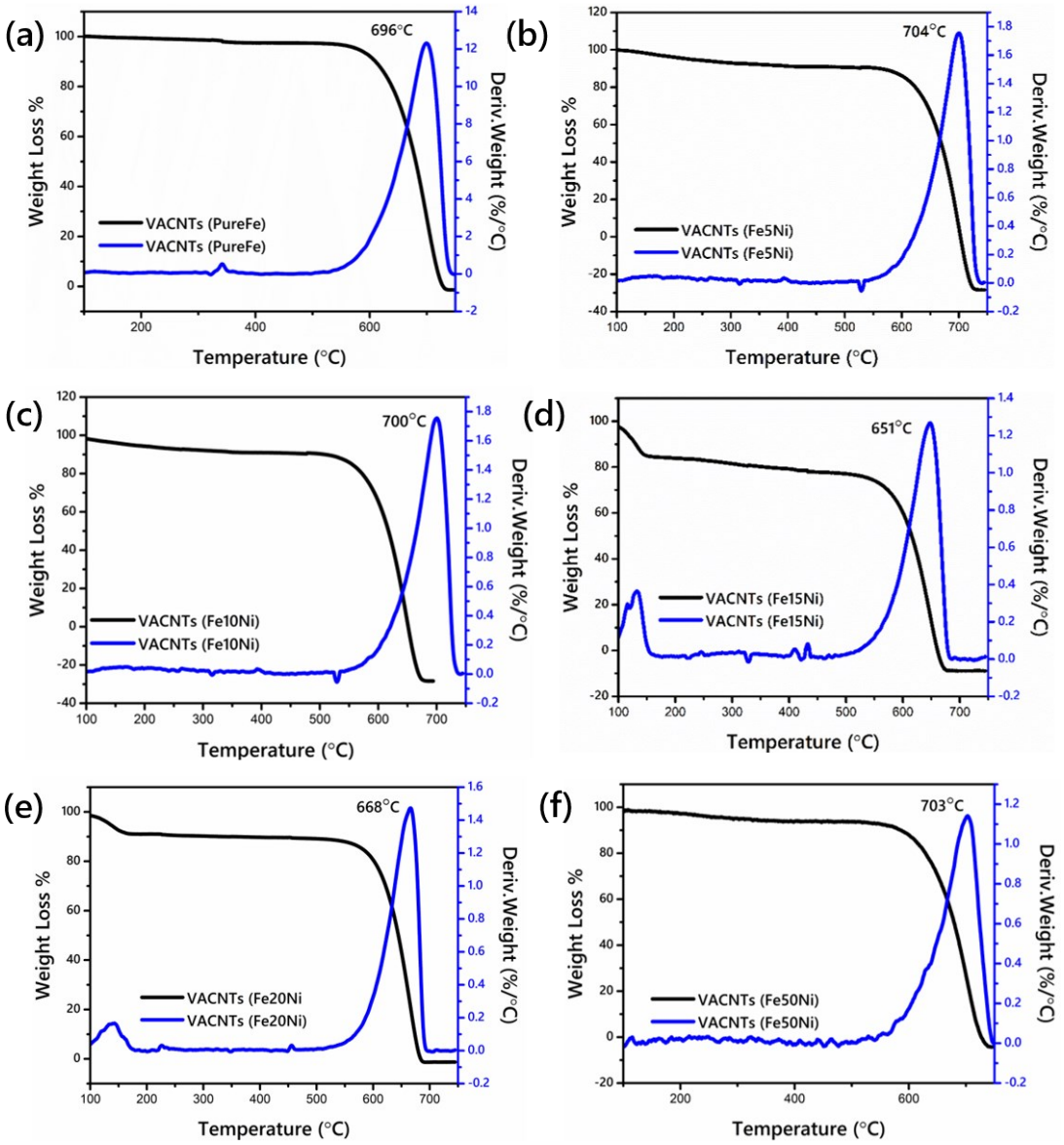

Fig.S 10: TGA curves of synthesized VACNTs on (a) pure-Fe, (b) Fe5Ni, (c) Fe10Ni, (d) Fe15Ni, (e) Fe20Ni and (f) Fe50Ni.